IEEE Access
Multidisciplinary ⋮ Rapid Review ⋮ Open Access Journal

Received December 9, 2019, accepted December 20, 2019, date of publication December 25, 2019, date of current version January 6, 2020.

Digital Object Identifier 10.1109/ACCESS.2019.2962300

Development of a Mathematical Model for Age-Dependent Radial Artery Pulse Wave Analysis Based on Pulse Waveform Decomposition

GWANGHYUN JO[1], TAE-HEON YANG[2], JAEUK U. KIM[3], JEONG-HOI KOO[4], AND YOUNG-MIN KIM[3]

[1]Department of Mathematics, Kunsan National University, Gunsan 54150, South Korea
[2]Department of Electronic Engineering, Korea National University of Transportation, Chungju 27469, South Korea
[3]Future Medicine Division, Korea Institute of Oriental Medicine, Daejeon 34054, South Korea
[4]Department of Mechanical and Manufacturing Engineering, Miami University, Oxford, OH 45056, USA

Corresponding author: Young-Min Kim (irobo77@kiom.re.kr)

This work was supported by a Grant from the Korea Institute of Oriental Medicine (KIOM), funded by the Korean Government under Grant KSN1911250.

ABSTRACT Radial artery pulse waveforms (RAPWs) have been actively studied for decades because they provide critical health information, particularly related to risk factors of cardiovascular disease. The primary goal of this study is to develop a novel mathematical model that can regenerate age-dependent RAPWs by decomposing a single pulse pressure waveform (PPW). This study proposes to decompose a PPW into three waveform components with one forward wave component and two reflected wave components based on the physiology of pulse waveforms. Treated as basis functions, the three components with associated control parameters are incorporated in the proposed mathematical model. The underlying idea of the model is to generate desired pulse waveforms by combining basis functions whose characteristics depend on selection of control parameter values. For the current study, after determining the nine control parameters of the basis functions by post-processing algorithms, the proposed model for the PPW is derived from a linear combination of the basis functions. Using the model along with *in vivo* RAPW data, this study evaluates the performance of the model in regenerating PPWs for a wide range of ages from 85 years old to 15 years old. The results show an error of less than 6% between the PPWs numerically derived from the model and the *in vivo* data for the two key matrixes used in this study (the least-square error norm and the radial augmentation index), validating the effectiveness of the model. The model is applicable for RAPW simulator analysis and development.

INDEX TERMS Age-dependent, hemodynamic, radial artery pulse waveform, wave decomposition, wave reflection model.

I. INTRODUCTION

Radial artery-pulse waveforms (RAPWs) have been investigated as a useful indicator for predicting the risk of cardiovascular diseases. This is mainly attributed to the benefits of RAPW measurements, which provide hemodynamic features (such as arterial stiffness, blood pressure, and cardiac output), the ease of access to the arteries, and comfortable measurement conditions [1]–[3]. Consisting of forward and backward waves, RAPWs can reveal valuable cardiovascular conditions. In particular, the wave reflection (the backward propagation of pulse pressure (PP) from the periphery to the heart) plays an important role in understanding aortic pathophysiology. Several studies report the importance of RAPWs and how they are affected by the conditions and properties of circulatory systems. Research work by Sugawara *et al.* [4] showed that the major reflection site of pressure waves shifts distally with aging, partly due to the closer matching

The associate editor coordinating the review of this manuscript and approving it for publication was György Eigner.

of impedance provided by central and peripheral arterial stiffness. In their study on circadian variation of wave reflections, Papaioannou *et al*. [5] reported that the morning-related amplification of wave reflections may have potential implications for the increased risk for cardiovascular events during the early morning. Meanwhile, Qasem and Avolio [6] evaluated a noninvasive method for estimating an aortic pulse wave velocity, one of the critical biomarkers of cardiovascular diseases, from a transformed RAPW and a waveform decomposition technique.

Recognizing the significance of the reflected waves in cardiovascular physiology, extensive studies focused on extracting the reflected waves from RAPWs. The wave intensity analysis is one of the most popular methods for decomposing pulse pressure and velocity waveforms [7]–[10]. However, to apply this decomposition method, one has to measure the velocity of the blood at the aortic vessel, which is a non-trivial procedure. Alternative to the wave intensity analysis methods, black box signal processing techniques are used to decompose waveforms, such as independent component analysis (ICA) [11], [12], and decomposition of photoplethysmographic arterial pulses via ICA, which is demonstrated in some studies [13], [14]. However, the signal processing algorithms are sensitive to the selection of parameters, and identifying optimal values is challenging. Other approaches include the use of several Gaussian functions to decompose aortic pulse pressure waveforms (PPWs) [15]–[17], and the wave reflection model analyses [18]–[20]. One of the oldest established theories, the wave reflection model analyses utilize the relationships between aortic PP and flow rate via the characteristic impedance and they are still used effectively. Central aortic PPW and flow rate waveform (FRW) are effectively decomposed by using the wave reflection model analyses in some references [6], [21], [22]. The strength of these wave reflection models is their ability to regenerate FRWs using derived control parameters as well as verify the accuracy of the reconstructed forward and reflected waves by matching hemodynamic characteristics. Aging is highly related to physiological changes in the cardiovascular system, affecting arterial pulse waveforms. Kelly *et al* studied age-related human arterial pulse waves with human subjects aged 2 to 91 [23]. In the case of radial pulses, they analyzed radial pulse waveforms of 420 subjects and showed that changes of the radial pulse characteristics were evident with aging. With increasing age, the fluctuations of the RAPWs were less distinct. Moreover, the peaks progressively come together, and their amplitudes were increased with advancing age. As aging occurs, distinct changes in arterial pulse waveforms take places. However, analyses of age-dependent RAPWs have been neglected. In spite of the effectiveness of wave reflection models, there have been little efforts to evaluate the performance of those models for analyzing RAPWs over a wide range of ages. This study proposes a new mathematical model for reconstructing age-related RAPWs based on the decomposition of a single PPW. It will use a mean pulse pressure waveform of 85-year-old people to regenerate RAPWs of various age groups.

TABLE 1. Demograhpics of the individuals included for the waveform analysis. The data are presented in mean ± standard deviation. BP: blood pressure in *mmHg*.

	Age 15	Age 35	Age 65	Age 85
Total (n)	68	356	584	10
Males (n)	30	184	293	5
Females (n)	38	172	291	5
Age (yr)	19.43±1.11	37.08±2.66	64.83±2.81	83.80±2.86
Height (cm)	166.53±8.16	168.44±7.93	161.01±8.31	156.81±9.31
Weight (kg)	60.03±9.37	65.00±14.17	63.47±9.96	60.02±12.96
Systolic BP	117.71±13.10	117.88±15.85	127.10±15.64	134.20±11.11
Distolic BP	65.49±8.50	72.13±9.64	75.54±10.91	79.10±6.28
Heart Beat	80.00±11.83	73.89±10.39	74.88±10.59	69.20±10.03

The primary goals of this paper are (1) to establish a new method to decompose a single PPW into one forward wave and two reflected waves, (2) to reconstruct RAPWs of a wide range of ages, (3) and to reconstruct the FRW, which can be used to effectively evaluate the reproduced pressure waveform in terms of hemodynamic characteristics.

The paper is organized as follows: the next section (section II) describes the mean RAWPs for various age groups. It will then present the process of the proposed mathematical model development. Details of the decomposition algorithms and the verification of the model are also provided in Section II. Next, the results and analysis of age-related RAWPs and FRWs are provided in Section III. Finally, the conclusion is presented in Section IV.

II. DATA PROCESSING AND WAVE DECOMPOSITION-BASED APPROXIMATION MODELING

RAPWs provide hemodynamically important information that can help predict the risk of cardiovascular disease, such as atherosclerosis, hypertension, and more. This study uses age-related RAPWs to investigate a new wave decomposition model. This section first describes how in vivo RAPWs are collected for a wide range of ages, from teenagers to the elderly. It then explains an overall modeling process to regenerate age-related RAPWs using a single PPW. Details of the modeling algorithms and rationales are also provided in this section.

A. DETERMINATION OF THE MEAN PULSE PRESSURE WAVEFORM BY AGE

The pulse data are collected from general individuals of Korean populations through health examinations and clinical study. The detailed demographics are as shown in Table 1. Physical information such as height, weight and heart beat was collected from tens to hundreds of subjects recruited for each age group. In particular, informative systolic and diastolic blood pressure for each age was recorded in the brachial artery of the upper arm.

This study uses age-dependent radial artery-pulse waveform data measured by a robotic tonometry system (RTS) device at the Korea Institute of Oriental Medicine [24]–[27]

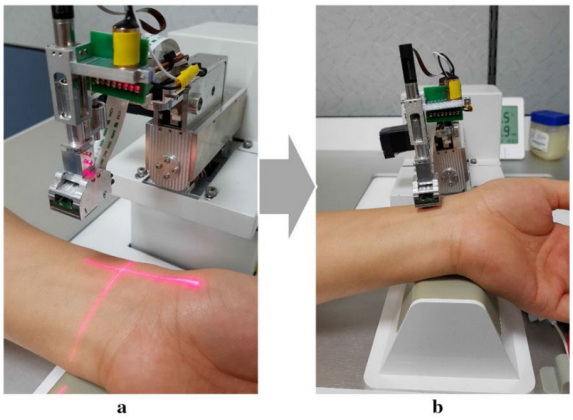

FIGURE 1. Measurements of in vivo radial pulse pressure waveforms by the robotic tonometry system (RTS): (a) the operator first takes the pulsation position with his/her fingers, identifies the radial artery in the wrist, and marks the pulsatile position using the laser pointer, (b) the RTS contacts the wrist and applies a proper hold-down pressure. The embedded pulse sensors at the tip of the RTS collect the RAWP data.

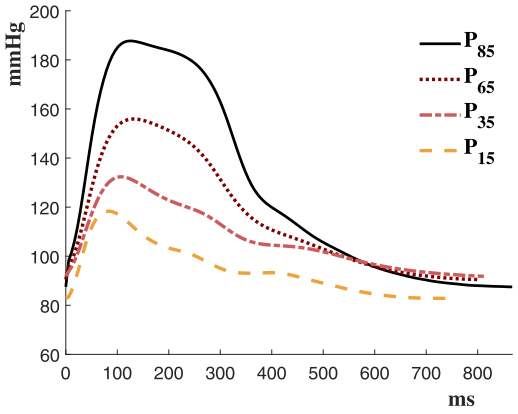

FIGURE 2. Mean radial pulse pressure waveforms for 15, 35, 65, and 85 year old age group.

(see Fig. 1). Based on the PPW data measured in the left radial artery from 1018 subjects aged 14 to 89 years, the average waveforms for 15, 35, 65, and 85 age groups were calculated by averaging the data centered-around with the age group with an interval of $\pm$ 5 years. The number of PPWs used for averaging were 68, 356, 584 and 10 for each of the age group, respectively. As depicted in Fig. 2, the average waveforms calculated show distinct waveform variations in terms of pulse pressure and augmentation index (AI), reflecting the effect of aging on pulse waveforms [23].

B. OVERALL MODELLING PROCESS

Fig. 3 describes the overall modeling process. As shown in Fig. 3 (a), the RAPW of the 85-year-old group is selected to decompose into forward and reflected waveforms. The selection of the 85-year-old's RAPW is based on the concept that the flow rate wave decreases as the pressure of the reflected wave increases along with an assumption that the flow rate waveform can be characterized as a triangular function. Next, by modifying the shape of FRW, the reflected waveform is decomposed into two reflected waveforms (see Fig. 3 (b)). By treating each of the waveform components as basis functions, P_1, P_2, and P_3, a function with control parameters for the basis functions (P_1, P_2, and P_3) can be given by

$$\widetilde{P}(t) = \sum_{i=1,2,3} w_i L_{k_i}\{P_i(t - t_i)\}. \tag{1}$$

where, w_i's are weighting parameters, k_i's are pulse broadening parameters, t_i's are phase delaying parameters, and L_k's are pulse broadening operators (see Fig. 3 (c)). This function, $\widetilde{P}(t)$, in (1) can be used to regenerate radial pulse pressure waveforms for each of the age groups by adjusting the control parameters.

For a target waveform P, representing one of the in vivo RAPWs, it is necessary to identify control parameters for the mathematical model's waveform $\tilde{P}$ to reconstruct the target age group's RAPW. Identifying the control parameters includes solving a minimization problem, which minimizes the difference between the target waveform (P) and the approximate waveform ($\widetilde{P}$) in terms of the of the least square norm and the radial AI, as in Fig. 3 (d). By an iterative process based on a line search method, the parameters are updated in each iteration to minimize the objective functions (see Fig. 3 (e)).

By piecewise-linearly interpolating the parameters w_i, k_i, and t_i from $age = 15$ to $age = 85$, the reconstructions of PPW for all age groups are obtained (see Fig. 3 (f)). Finally, validation of the PPW approximation modeling is conducted (see Fig. 3 (g)), through relative error analyses of least square, AI, and max value error. In addition, the reconstruction of FRW which can be easily obtained from the proposed approximation modeling are presented.

C. DECOMPOSITION OF THE PULSE PRESSURE'S FORWARD AND REFLECTED WAVES

Based on the physiological characteristics, it is well known that arterial pulse waveforms are comprised of forward and reflected waves. In order to decompose a central aortic pressure waveform, Qasem and Avolio [6] separated it into forward and reflected waves using an uncalibrated triangular aortic flow waveform. In their analytic study, the measured time-varying pulse pressure wave, P, was expressed as a sum of forward (P_f) and reflected (P_b) waves as described in (2a). Since the flow rate, Q, decreases as the pressure of the reflected wave increases, the flow rate is expressed as the difference between the forward flow rate (Q_f) and the reflection flow rate (Q_b) as shown in (2b). From the transmission line analysis, P_f and P_b were obtained from P, Q, and the characteristic impedance, Z_c, as shown in (2c) and (2d).

$$P = P_f + P_b \tag{2a}$$

$$Q = Q_f - Q_b \tag{2b}$$

$$P_f = \frac{P + Z_C Q}{2} \tag{2c}$$

$$P_b = \frac{P - Z_C Q}{2}. \tag{2d}$$

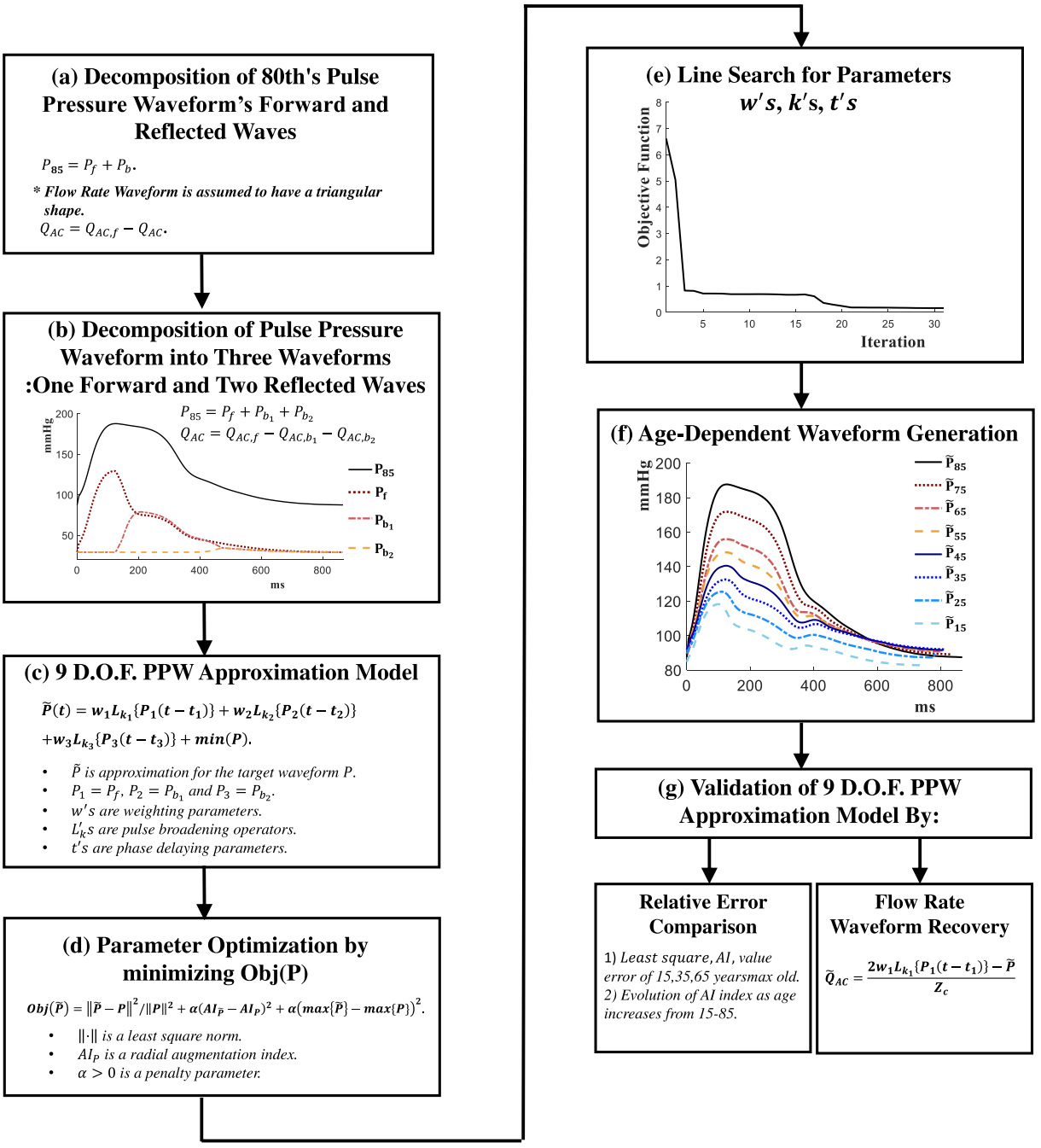

FIGURE 3. Illustration of the overall process.

In a physical sense, the flow rate is a fluctuating wave, consisting of AC and DC components. Hence, the flow rate can be expressed as $Q = Q_{AC} + Q_{DC}$, where Q_{DC} is the minimum DC-offset values of Q. The AC component for the flow rate contains more significant information of the FRW than the DC offset of the flow rate. Under this assumption, (2b)-(2d) are changed to (3a)-(3c).

$$Q_{AC} = Q_{AC,f} - Q_{AC,b} \tag{3a}$$

$$P_f = \frac{P + Z_C Q_{AC}}{2} \tag{3b}$$

$$P_b = \frac{P - Z_C Q_{AC}}{2}. \tag{3c}$$

FRWs are often assumed to be triangular functions in previous studies [6], [21], [22]. This study also defines Q_{AC} as a triangular model. As shown in Fig. 4, the triangular model for the FRW linearly increases from time $T = 0$ to its peak value at $T = T_1$, and linearly decreases to zero at $T = T_2$. In the model, the time T_1 is chosen based on the global maximum of P_{85} (the RAPW of 85-year-old), and the time T_2 is determined based on the point where the second derivative of P_{85} starts to decrease rapidly. Let us explain more about the relationships between Q_{AC} and Z_C. Noting that the maximum value of Q_{AC} and Z_C are multiplied in (3b) and (3c), one

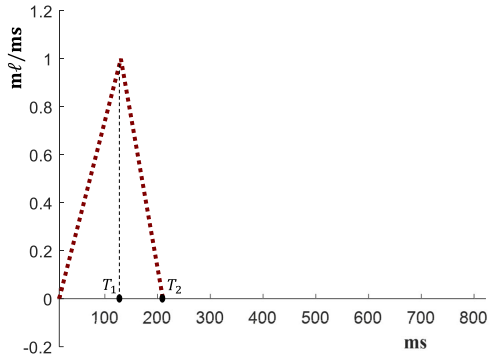

FIGURE 4. Initial estimation of the flow rate.

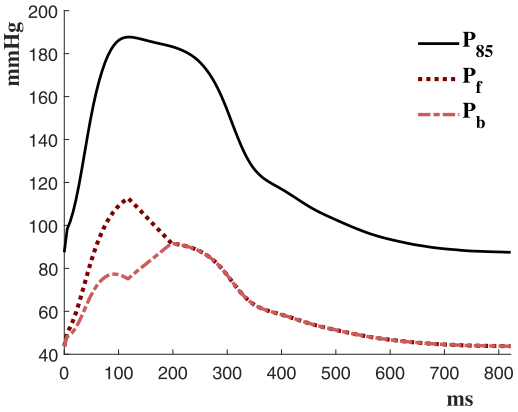

FIGURE 5. Wave decomposition by two parts (before applying ***PPP***).

may treat $max\{Q_{AC}\} \times Z_C$ as one variable Z'_C by assuming that $max\{Q_{AC}\} = 1\, m\ell/ms$. In the decomposition procedure, the real value of $max\{Q_{AC}\}$ does not affect the algorithms as long as the new variable Z'_C is reasonable. For the flow rate recovery procedure, which is discussed in the following section, we will find real values for Z_C such that the average of the resulting Q fits the average of the measured FRW. Let us explain the choice of Z'_C. Clearly, the parameter Z'_C should not be larger than the maximum value of P_{85}; otherwise, (3c) will produce P_b with negative values in some regions. On the other hand, if the value of Z'_C is too small, there will be only a small difference between P_f and P_b, which would make the decomposition algorithm meaningless. Noting that both P_{85} and Q_{AC} reach the maximum values at T_2, the assumption $max\{Q_{AC}\} = 1$, and (3b), we can show that

$$\begin{aligned} max\{P_f\} &= max\{P_{85} + Z'_C Q_{AC}\}/2 \\ &= P_{85}(T_2)/2 + Z'_C Q_{AC}(T_2)/2 \\ &= (max\{P_{85}\} + Z'_C)/2, \end{aligned}$$

implying that the choice of Z'_C determines the maximum value of P_f. For example, if we choose

$$Z'_C = \gamma max\{P_{85}\}, \tag{4}$$

for some $0 < \gamma < 1$, then,

$$max\{P_f\} = \frac{1+\gamma}{2} \times max\{P_{85}\}.$$

In this work, Z'_C is chosen as approximately 40% of the maximum value of P_{85}. If Z'_C is changed with $0.3 < \gamma < 0.5$ in (4), magnitudes of the waveform P_f and P_b change, but the shapes of the waveforms are similar. Because we will normalize P_f and P_b in the proposed mathematical model in (1), the choices of γ between the range (0.3, 0.5) have small effects on the performance of the proposed model.

Fig. 5 shows P_f and P_b waveforms before applying the post processing procedure along with P_{85}. The waveform Pf and Pb are obtained by substituting the value of P_{85} and Q_{AC} (assumed to be triangular) in (3b) and (3c). As shown in the figure, the waveforms P_f and P_b show nonsmooth shapes because Q_{AC}, whose gradient changes abruptly, was subtracted from P_{85}. Thus, we apply the following post-processing procedure to make the waveform of P_f and P_b smooth.

Post Processing Procedure (PPP)*: The post processing procedure can be summarized as:* $(P'_1, P'_2) = \boldsymbol{PPP}(P_1, P_2, a, b)$ *Given the waveforms* P_1 *and* P_2 *and scalar values* $0 < a < b$*, we find the smooth waveforms* P'_1 *and* P'_2 *such that the following are satisfied:*

$$\frac{\partial P'_2}{\partial t} = 0, \quad 0 \le t \le a \tag{5}$$

$$\frac{\partial P'_1}{\partial t} < 0, \quad a \le t \le b \tag{6}$$

$$P'_1 + P'_2 = P_1 + P_2. \tag{7}$$

Let us explain each step of the ***PPP***. Firstly, (5) ensures that there is no (or meaningless) reflection between the start of systolic ejection and the peak of P_{85}. The condition in (6) is imposed to reflect that the forward pressure wave decreases at the arrival of the reflected pressure wave. Finally, (7) guarantees that the sum of reflected waveform and forward waveform is equal to P_{85}. After applying this ***PPP*** to P_f and P_b, i.e., $(P_f, P_b) = \boldsymbol{PPP}(P_f, P_b, T_1, T_2)$, the final waveforms P_f and P_b have smooth shapes with only one local peak, as shown in Fig. 6.

D. DECOMPOSITION OF PPW INTO THREE WAVEFORMS: ONE FORWARD AND TWO REFLECTED WAVES

In this study, a new algorithm is proposed to decompose PPWs using three waveforms (one forward and two reflected waves). In the proposed algorithm, P_b is decomposed into two reflected waves (P_{b_1} and P_{b_2}). This subsequently introduces Q_{AC,b_1} and Q_{AC,b_2}, satisfying the decomposition $Q_{AC,b} = Q_{AC,b_1} + Q_{AC,b_2}$. Substituting $P_b = P_{b_1} + P_{b_2}$ and $Q_{AC,b} = Q_{AC,b_1} + Q_{AC,b_2}$ in (2a) and (3a), one obtains the following equations:

$$\begin{aligned} P &= P_f + P_{b_1} + P_{b_2} \\ Q_{AC} &= Q_{AC,f} - Q_{AC,b_1} - Q_{AC,b_2}. \end{aligned} \tag{8}$$

To develop a new algorithm, the previously used triangular model for the FRW must be modified. To this end, a new

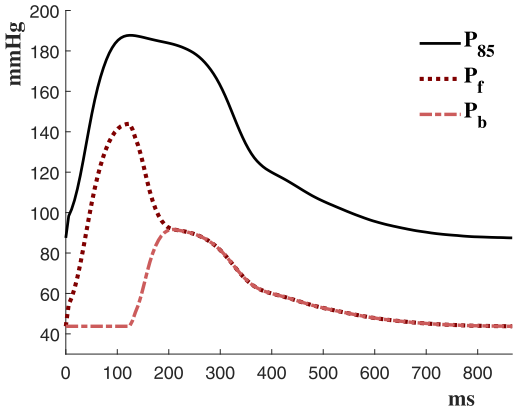

FIGURE 6. Wave decomposition by two parts (after applying ***PPP***).

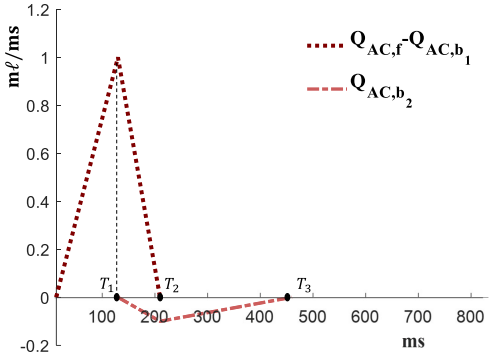

FIGURE 7. Illustration of the modified initial estimation for Q_{AC}, which is the sum of the positive region ($Q_{AC,f} - Q_{AC,b_1}$) and the negative region (Q_{AC,b_2}).

triangular function with a negative magnitude is added to the previous triangle model (see Fig. 7). The "negative" triangle model is needed to account for the new reflection wave Q_{AC,b_2} and the negative region corresponds to Q_{AC,b_2}. Owing to (8) and the fact that the negative triangle corresponds to Q_{AC,b_2}, the positive triangle corresponds to the difference between Q_{AC} and Q_{AC,b_2}.

Let us describe the newly added triangle (Q_{AC,b_2}) in more details. The triangle starts at time $T = T_1$ and reaches to its peak value at $T = T_2$. It then ends at $T = T_3$. The height of the new triangle is set to 10% of the positive region to reflect that the second reflection of P only has a small influence on flow rate. The time T_3 is the location on the horizontal axis where the absolute value of the second derivative of P_{85} starts to decrease.

Following the illustration of Q_{AC}, mathematical expressions of the proposed decomposition for P_b are explained. The notation P_{b_1} is used for the first reflected waveform and P_{b_2} is used for the second reflected waveform where the magnitude of P_{b_1} is larger than that of P_{b_2}. Note that the properties of P_{b_1} and P_{b_2} may satisfy the following conditions: 1) the sum of P_{b_1} and P_{b_2} should be equal to P_b, 2) there exists coefficient β such that

$$P_{b_1} - P_{b_2} \approx \beta Q_{AC,b_2}. \tag{9}$$

The second property is motivated by the fact that the second reflected pulse pressure (P_{b_2}) produces the second reflected flow rate (Q_{AC,b_2}). Thus, determining a reasonable coefficient β is crucial in the decomposition process. To find such β, note that P_b is written as

$$P_b = \frac{P - Z_C' Q_{AC}}{2} = \frac{P - Z_C'(Q_{AC,f} - Q_{AC,b_1} - Q_{AC,b_2})}{2}, \tag{10}$$

by assigning the Q_{AC} value defined in (8) to the Q_{AC} value in (3c). By separating the last term ($Z_C' Q_{AC,b_2}/2$) in (10), which is related to the effect of the second reflection on the flow rate, we can introduce the following expressions

$$P_{b_1} = \frac{P - Z_C'(Q_{AC,f} - Q_{AC,b_1})}{4} + \left(\frac{1}{4} + \rho\right) Z_C' Q_{AC,b_2}, \tag{11}$$

$$P_{b_2} = \frac{P - Z_C'(Q_{AC,f} - Q_{AC,b_1})}{4} + \left(\frac{1}{4} - \rho\right) Z_C' Q_{AC,b_2}, \tag{12}$$

for some parameter $\rho > 0$. Note that the relationship (11) and (12) satisfies the properties 1) and 2) above when $\beta = 2\rho Z_C'$ in (9). This formulation reflects that the difference between P_{b_1} and P_{b_2} is proportional to Q_{AC,b_2}. In other words, in the absence of Q_{AC,b_2}, no further reflection waveform is produced. In the decomposed reflection waveform equations, the parameter ρ plays the role of controlling the weights for the characteristic impedance coefficient, i.e., as ρ gets larger, P_{b_1} gets larger and P_{b_2} gets smaller. In this work, this parameter is chosen to be $\rho = 1/2$. This choice results in $\beta = Z_C'$ in (9), i.e., $P_{b_1} - P_{b_2} = Z_C' Q_{AC,b_2}$. In other words, the scale of the characteristic impedance Z_C' remains the same. When a large value of ρ is chosen ($\rho > 1$), the magnitude of P_{b_2} would be too small, making the post processing of the basis functions challenging. However, other choices of ρ gives similar decomposition results when $1/4 < \rho < 1$. From (10)-(12), the resulting decompositions are formulated as

$$P_{b_1} = \frac{P_b + Z_C' Q_{AC,b_2}}{2}, \tag{13}$$

$$P_{b_2} = \frac{P_b - Z_C' Q_{AC,b_2}}{2}. \tag{14}$$

The new decomposition (three-component decomposition of PPW) algorithm is summarized next. The proposed algorithm has two parts. The first part decomposes P into P_f and P_b with similar techniques described earlier and the 2^{nd} part of algorithm involves with the decomposition of P_b into P_{b_1} and P_{b_2}. During the 2^{nd} part of the algorithm, the post processing of P_{b_1} and P_{b_2} must be performed to complete the three-component decomposition of pulse pressure waveforms, obtaining smooth P_f, P_{b_1} and P_{b_2}.

Algorithm 1. Three-component decomposition of PPW.

1) *Decompose of P into two parts, P_f and P_b.*
   a) *Substitute P and Q_{AC} to (3b) and (3c) to obtain P_f and P_b.*
   b) *(Post processing) Perform the process*
   $$(P_f, P_b) = \boldsymbol{PPP}(P_f, P_b, T_1, T_2),$$

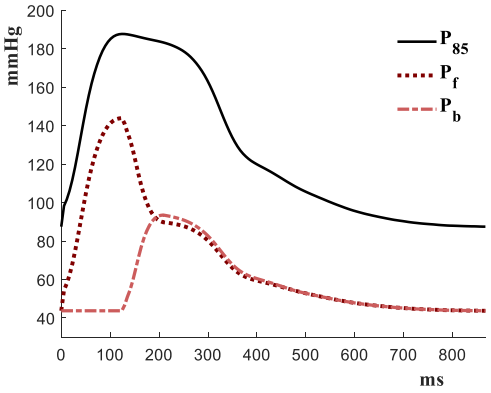

(a) After first step in ***Algorithm 1***.

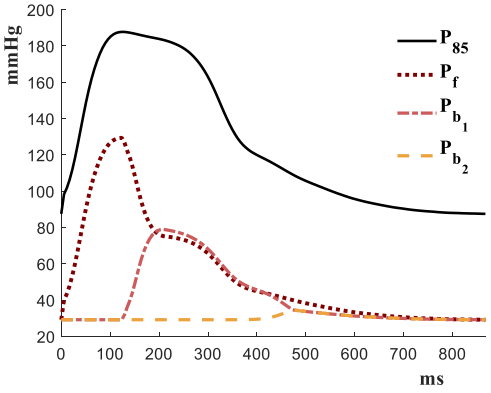

(b) Final results of ***Algorithm 1***.

FIGURE 8. Decomposition of PPW at age 85 via ***Algorithm 1***.

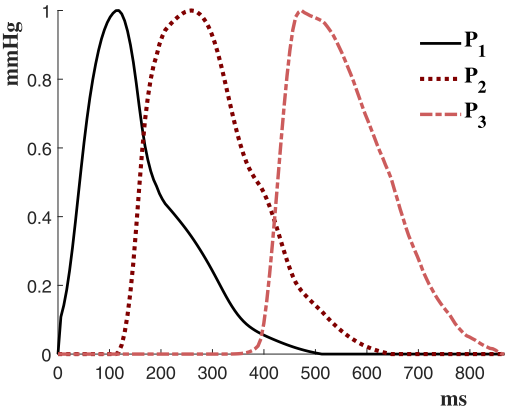

FIGURE 9. Basis functions P_1, P_2 and P_3.

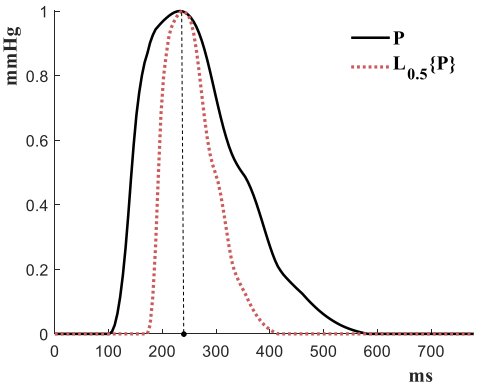

FIGURE 10. Example of operator L_k where $k = 0.5$. The shape of P is narrowed uniformly with respect to the local peak of P.

2) *Decompose of P_b into P_{b_1} and P_{b_2}.*
   a) *Substitute P_b and Q_{AC,b_2} to (13) and (14) to obtain P_{b_1} and P_{b_2}.*
   b) *(Post processing) Perform the process*
   $$(P_{b_1}, P_{b_2}) = \boldsymbol{PPP}(P_{b_1}, P_{b_2}, T_2, T_3).$$

Fig. 8 shows the decomposition of P_{85} using the proposed algorithm. Fig. 8 (a) shows P_f and P_b obtained by the first step. The final three components obtained after the post processing are shown in Fig. 8 (b).

E. PPW APPROXIMATION MODEL

This section introduces a new approximation model based on the three decomposed waveforms by the proposed algorithm as basis functions to reconstruct PPWs. Once a target PPW is decomposed by ***Algorithm 1***, the waveforms of P_f, P_{b_1} and P_{b_2} are used as basis functions. These basis functions along with their control parameters are what defines the skeleton model. In order to enhance the flexibility of the model, the basis functions have been slightly modified such that the resulting functions (say P'_f, P'_{b_1}, and P'_{b_2}) have the duration of 500 *ms* or less and

$$P_{85} = P_f + P_{b_1} + P_{b_2} = P'_f + P'_{b_1} + P'_{b_2}.$$

Here, the heights of the modified functions P'_f, P'_{b_1}, and P'_{b_2} are 99.68, 56.59 and 10.17, respectively. The functions are then normalized so that they each have a height of 1 (see Fig. 9). For simplicity, the resulting waveforms are written as P_1, P_2 and P_3, where each waveform is obtained from P_f, P_{b_1} and P_{b_2}, respectively. Consequently, the P_i's $(i = 1, 2, 3)$ are constructed so that the following linear combinations produce the exact graph of P_{85}:

$$P_{85} = 99.68P_1 + 56.59P_2 + 10.17P_3 + min(P_{85}), \quad (15)$$

where $min(P_{85}) = 87.72$.

Now, let us describe how the new model is used to reconstruct the target PPW. Given a target P, the approximation $\tilde{P}_{85}$ is expressed by the three basis functions P_i's, $(i = 1, 2, 3)$ together with nine parameters w_1, w_2, w_3, k_1, k_2, k_3, t_1, t_2 and t_3:

$$\begin{aligned}\widetilde{P}(t) = w_1 L_{k_1}\{P_1(t - t_1)\} + w_2 L_{k_2}\{P_2(t - t_2)\} \\ + w_3 L_{k_3}\{P_3(t - t_3)\} + min(P). \quad (16)\end{aligned}$$

In the model above, t_1, t_2, and t_3 play the role of the linear transportation (or delay) of the basis functions P_1, P_2, and P_3, respectively. The operator L_k is a broadening operator for the basis functions. $L_k\{P\}$ broadens the shape of P with respect to the location of the peak of P. For example, if $k = 1$, $L_k\{P\} = P$ (no broadening). For $k = 0.5$, the support of $L_k\{P\}$ becomes half of P while maintaining the same shape (see Fig. 10). If $k > 1$, the shape of $L_k\{P\}$ is uniformly widened. Finally, the weighting factors (w_1, w_2 and w_3) are used in the linear combination of $L_{k_1}\{P_1\}$, $L_{k_2}\{P_2\}$ and $L_{k_3}\{P_3\}$. For example,

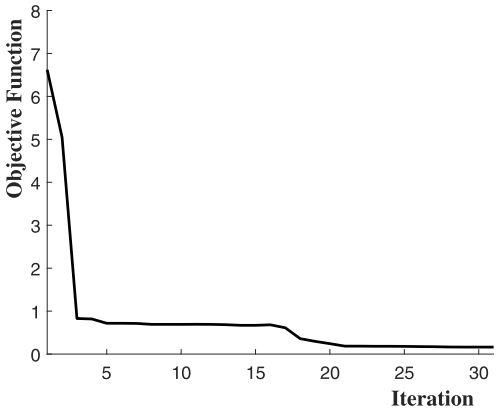

FIGURE 11. Evolution of objective function $Obj(\widetilde{P}_{15})$.

the expression in (15) can be viewed as the exact approximation of P_{85} using parameters $w_1 = 99.68$, $w_2 = 56.59$, $w_3 = 10.17$, $k_1 = k_2 = k_3 = 1$ and $t_1 = t_2 = t_3 = 0\,ms$.

To obtain optimal parameters for the approximation model, an optimization problem can be established. Given a target P, the objective function can be defined, which contains the least square error, the radial AI error and the maximum value error:

$$Obj(\widetilde{P}) = ||\widetilde{P} - P||^2 + \alpha(AI_{\widetilde{P}} - AI_P)^2 + \alpha(max\{\widetilde{P}\} - max\{P\})^2.$$

Here, $||\cdot||$ stands for least square norm (L_2-norm),

$$||P|| = \sqrt{\int_T P^2 ds},$$

and the radial AI of P is defined as

$$AI_P = \frac{Late\ Systolic\ Pressure\ from P}{Early\ Systolic\ Pressure\ from P}.$$

The parameters in (16) are defined such that the objective function is minimized.

$$(\mathbf{w}, \mathbf{k}, \mathbf{t}) = argmin_{(\mathbf{w},\mathbf{k},\mathbf{t})} Obj(\widetilde{P}), \tag{17}$$

where $\mathbf{w}_i = (w_1, w_2, w_3)$, $\mathbf{k} = (k_1, k_2, k_3)$ and $\mathbf{t} = (t_1, t_2, t_3)$. The parameter $\alpha > 0$ in $Obj(\widetilde{P})$ plays the role of the penalty parameter for radial AI and maximum value of $\widetilde{P}$, i.e., as α increases, the solution for (17) will minimize the difference of AI (and the maximum) value between P and $\widetilde{P}$. In this study, the parameter α was chosen to be 40. When the parameter gradually increases starting at $\alpha = 40$, given the minimizing problem (17), the difference between P's AI and reconstructed $\widetilde{P}$'s AI becomes smaller, while the L^2-error between P and $\widetilde{P}$ becomes too large. On the other hands, if α was smaller than 40, AI index of the reconstructed $\widetilde{P}$ was not accurate. We note that $w_1\ L_{k_1}\{P_1(t - t_1)\}$, $w_2\ L_{k_2}\{P_2(t - t_2)\}$ and $w_3\ L_{k_3}\{P_3(t - t_3)\}$ are approximations of the forward wave, the first reflected wave, and the second reflected wave of the PPW, respectively.

Let us describe the fitting process to solve (17) for the target waveform P_{65} (the process for the rest of age groups is similar). It is important to find reasonable initial guesses for the $\mathbf{w}^{(0)} = (w_1^{(0)}, w_2^{(0)}, w_3^{(0)})$, $\mathbf{k}^{(0)} = (k_1^{(0)}, k_2^{(0)}, k_3^{(0)})$ and $\mathbf{t}^{(0)} = (t_1^{(0)}, t_2^{(0)}, t_3^{(0)})$ to minimize the objective function. The initial guesses for w_i's are obtained from the weights in (15), i.e., $w_1^{(0)} = 99.68$, $w_2^{(0)} = 56.59$ and $w_3^{(0)} = 10.17$, since the waveforms P_{65} and P_{85} are similar. For the time delay parameters, the initial guesses were chosen to be $t_1^{(0)} = t_2^{(0)} = t_3^{(0)} = 0$. The initial guesses for the broadening parameters were chosen to be $k_1^{(0)} = k_2^{(0)} = k_3^{(0)} = 1$.

After selecting reasonable initial values for the control parameters, using an iterative method based on a line search, they were updated in each iteration step to minimize the objective function. This parameter fitting process was divided into two steps to avoid non-physiological solutions. Firstly, (17) was solved with $\alpha = 0$ using the iterative method based on a line search starting from $\mathbf{w}^{(0)}$, $\mathbf{k}^{(0)}$ and $\mathbf{w}^{(0)}$, resulting the parameters $\mathbf{w}^{(1)}$, $\mathbf{k}^{(1)}$ and $\mathbf{t}^{(1)}$. The obtained parameters $\mathbf{w}^{(1)}$, $\mathbf{k}^{(1)}$ and $\mathbf{t}^{(1)}$ are then used to determine the final parameters $\mathbf{w}^{(2)}$, $\mathbf{k}^{(2)}$ and $\mathbf{t}^{(2)}$ which are obtained by solving (17) with $\alpha = 40$. Fig. 11 shows the evolution of the objective function of $\widetilde{P}_{15}$ for each iteration step.

One of the benefits of the proposed approximation model is that the FRW can be recovered from the PPW once the parameters $\mathbf{w}$, $\mathbf{k}$ and $\mathbf{t}$ are determined. The following algorithm summarizes the flow rate recovery process.

Algorithm 2. Flow Rate Recovery Process.

1) *Compute the AC part of* $\widetilde{Q}$ *by*

$$\widetilde{Q}_{AC} = \frac{2w_1 L_{k_1}\{P_1(t - t_1)\} - \widetilde{P}}{Z_c}. \tag{18}$$

2) *Compute the DC part of* $\widetilde{Q}$ *by*

$$\widetilde{Q}_{DC} = \frac{\widetilde{P}_{ave}}{Z_c}.$$

where $\widetilde{P}_{ave}$ is the average of $\widetilde{P}$ over one period.

3) $\widetilde{Q} = \widetilde{Q}_{AC} + \widetilde{Q}_{DC}$.

Eq. (18) is derived from (3b) along with the fact that $w_1\ L_{k_1}\{P_1(t - t_1)\}$ is an approximation for the forward wave of the target PPW. It is noteworthy that Z_C is used in ***Algorithm 2*** not Z_C'. The values of Z_C for $age = 15, 35, 65, 85$ are provided in the results section.

III. RESULTS AND DISCUSSION

A. APPROXIMATION OF THE PPW FOR AGES 15, 35, AND 65

In this subsection, we present the approximation capability of the proposed mathematical model (16) which reconstructs the age-related RAPWs by a linear combination of three basis functions. The validation was focused on the ability of the model to describe waveforms of different ages by controlling the basis functions. In order to evaluate the performance of the model, the differences of the numerically derived PPWs and the *in vivo* PPW data were compared in terms of least-square norm, radial AI, and maximum values.

Table 2 summarizes optimal values of the three parameters, w_i, k_i, and t_i, that are obtained by solving the minimization problem in (17) for ages 15, 35, 65, and 85.

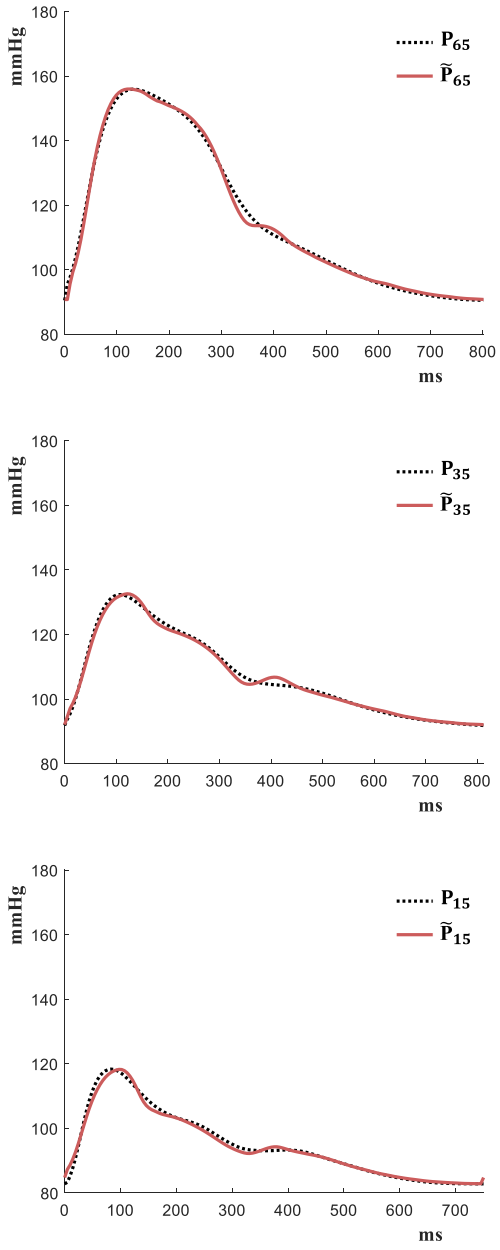

FIGURE 12. Comparison of P_{age} with $\tilde{P}_{age}$ for $age = 15$, 35, and 65.

The results show that all the weighting parameters, w_1, w_2, and w_3, increase as the age increases. This is because the maximum value of the PPW grows with increasing age. For the time delay related parameter t_i, the difference $t_2 - t_1$, decreases as the age increases. This result coincides with the analysis of [28] that the reflected wave travels faster with increasing age.

By applying the optimized values to the approximation model, age-related pulse waveforms (P_{age}) can be reconstructed. Fig. 12 compares the absolute differences between the real values (P_{age}) and the estimation values ($\widetilde{P}_{age}$) of the average pulse waveform for $age = 15$, 35, and 65. In order to evaluate the performance of the approximation model, three

TABLE 2. Errors from the three-waveform decomposition for $age = 15$, 35, 65, and 85.

Age	$w_i, (i = 1, 2, 3)$	$k_i, (i = 1, 2, 3)$	$t_i, (i = 1, 2, 3)$
15	35.383	0.857	$-2.106\ ms$
	7.207	1.264	$50.131\ ms$
	5.842	0.826	$-13.902\ ms$
35	40.374	0.966	$6.385\ ms$
	12.460	1.029	$13.683\ ms$
	8.150	1.100	$-10.490\ ms$
65	65.135	0.924	$5.850\ ms$
	33.539	0.893	$5.850\ ms$
	9.963	1.050	$-2.700\ ms$
85	99.681	1.000	$0.000\ ms$
	55.383	1.000	$0.000\ ms$
	10.173	1.000	$0.000\ ms$

TABLE 3. Errors from the three-waveform decomposition for $age = 15$, 35, 65, and 85.

Age	Relative L^2-error	Relative AI error	Relative max error
15	5.88%	5.97%	0.13 %
35	4.56%	0.45%	0.63 %
65	3.43%	1.53%	$8.77{\cdot}10^{-2}$%
85	0.00%	0.00%	0.00%

TABLE 4. Errors from the two-waveform decomposition for $age = 15$, 35, 65, and 85.

Age	Relative L^2-error	Relative AI error	Relative max error
15	15.14 %	24.60%	0.43%
35	14.29%	30.79%	3.99 %
65	5.93%	$1.16{\cdot}10^{-2}$%	$2.19\cdot10^{-2}$%
85	0.00%	0.00%	0.00%

kinds of errors are considered. First, one is the relative L^2-norm, i.e.,

$$\frac{||\widetilde{P}_{age} - P_{age}||}{||P_{age}||}.$$

The second is the relative AI error, and the last is the relative max error.

Table 3 shows the errors between P_{age} and $\widetilde{P}_{age}$ for $age = 15, 35, 65$, and 85. As shown in Table 3, the maximum relative L^2 error across all ages is 5.88%. For the relative AI and maximum error values, the maximum errors are 5.97% and 0.63%, respectively.

To assess the performance of the proposed approximation model based on three-component waveforms, the same error analyses are conducted for the two-component-based approximation model, which consists of one forward wave and one reflected wave. Given a targeted P, the two components-based approximation $\widehat{P}(t)$ is given by

$$\widehat{P}(t) = w_1\, L_{k_1}\{P_1^*(t - t_1)\} + w_2\, L_{k_2}\{P_2^*(t - t_2)\} + min(P),$$

where P_1^* and P_2^* are the forward and reflected waveforms, respectively. The parameters are determined by solving the same minimization problem shown in (17).

Table 4 shows the results for the two-waveform decomposition model. The L^2 errors of the two components-based model are over 14% for $age = 15$ and 35, indicating that the error between the target PPW and the approximated PPW is substantial. Furthermore, the AI errors are over 24% when $age = 15$ and 35. Thus, it is clear that the three-component model outperforms the two-component model in

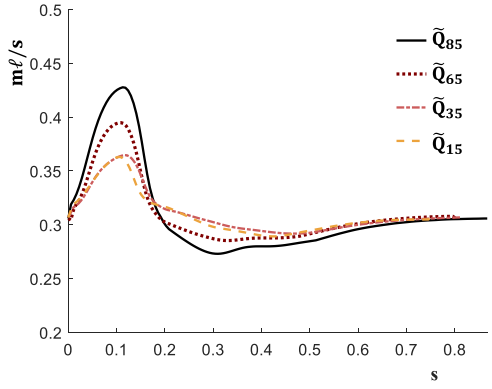

FIGURE 13. Recovered FRW for *age* = 15, 35, 65, and 85.

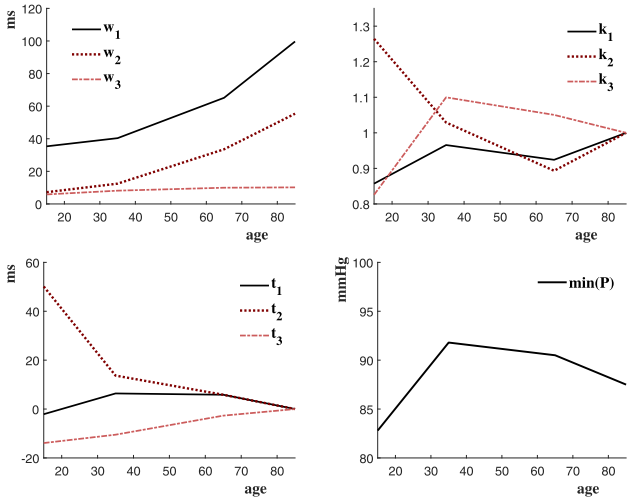

FIGURE 14. Evolution of parameters, **w**, **k**, **t**, ***min*(*P*)**, for (16) for age between 15 and 85.

accurately approximating target pulse pressure waveforms. In other words, the decomposition of the reflected waveform is required for better approximation of the PPW for all ages. It is expected that more than three decompositions could enhance the accuracy of the approximation model. Therefore, we expect to develop a generalized decomposition algorithm for the reflected waveforms and to resolve the optimum parameters for the decomposed reflected waves in a future work.

B. FRW RECOVERY FOR AGES 15, 35, 65, AND 85

In ***Algorithm 2***, the values of Z_C affect the minimum, maximum, and average values of Q. This implies that Z_C can be determined as long as the average of the FRW is known.

The average flow rate in a radial artery can be computed using the following formula:

$$Flow\ Rate = \pi(Diameter/2)^2 \cdot (Velocity).$$

The diameter of the right and left radial arteries was measured as $2.3 \pm 0.4\ mm$ and $2.2 \pm 0.4\ mm$, respectively, in [29]. The blood velocity of the right and left radial arteries was measured as $7.2(4.2 - 10.2)\ cm/s$ and $8.8(6.6 - 11.3)\ cm/s$, respectively, in [30]. Thus, using these published data, the

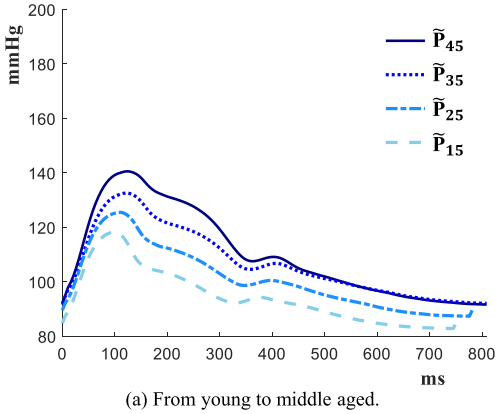

(a) From young to middle aged.

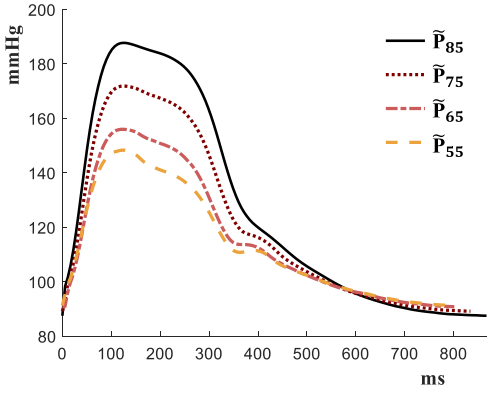

(b) From middle to older aged.

FIGURE 15. Approximation of PPW for *age* = 15, 25, 35, . . . , 85.

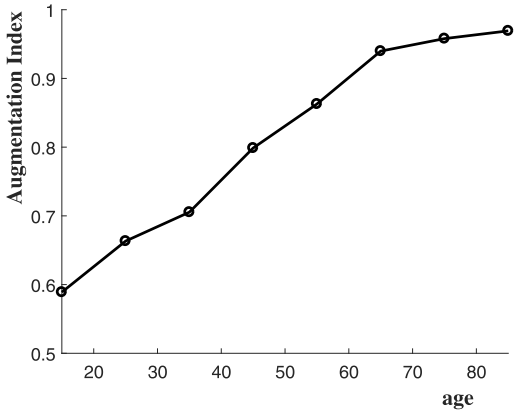

FIGURE 16. Radial AI of $\widetilde{P}$.

average flow rate can be computed as $3.14 \cdot (1.125\ mm)^2 \cdot 8.0\ cm/s = 0.31\ m\ell/s$. By finding Z_C such that the resulting $\widetilde{Q}$ has an average value of $0.31\ m\ell/s$, Z_C for *age* =15, 35, 65, and 85 can be calculated. Table 5 shows the values of Z_C and resulting average of flow rate. The results show that the characteristic impedance in the radial artery increases with increasing age. This trend corresponds to the behavior of characteristic impedance in the central artery.

Fig. 13 shows the recovered FRWs by ***Algorithm 2*** for *age* = 15, 35, 65, and 85.

TABLE 5. Characteristic impedance and average of the FRW for *age* = 15, 35, 65, and 85.

Age	$Z_c(mmHg \cdot ms/m\ell)$	Average of $\widetilde{Q}_{AC}(m\ell/s)$
15	311	0.31
35	349	0.31
65	378	0.31
85	413	0.31

C. APPROXIMATION OF PPW FOR ALL AGES

By piecewise-linearly interpolating the parameters **w**, **k**, **t** and $min(P)$ from $age = 15$ to $age = 85$, the PPW can be reproduced for all ages between 15 and 85 by substituting these parameters into (16). Fig. 14 shows the evaluation of parameters **w**, **k**, **t** and $min(P)$ for the age group considered in this study. Fig. 15 shows the approximated PPWs for $age = 15, 25, ..., 85$. While Fig. 15 (a) shows reproduced PPWs of the young to middle ages, from 15 to 45 year old with an increment of a decade, those of the ages from 55 to 85 year old with an increment of 10 years are shown in Fig. 15 (b).

Fig. 16 shows the variation of radial AIs as the age varies from 15 to 85-year-olds. As shown in the figure, the radial AI increases as the age increases. Furthermore, with increasing age, the radial AI linearly increases but plateaus at approximately 60-year-old. This result is similar to the age-related changes in central aortic stiffness reported in a group of South Asian individuals [31].

IV. CONCLUSION

This study has developed a novel mathematical model for analyzing RAPWs at all ages. It validated the performance of the model in reproducing age-related pulse pressure waveforms with in-vivo RAPW data. The approximation model is developed based on three decomposed components of the 85-year-old PPW and nine control parameters of the decomposed waveforms. Solving the minimization problem, the optimal parameters of the approximation model were determined for age 15, 35, and 65. The effects of the model parameters were investigated with aging. As the age increases, the weight-related parameters increase uniformly and the time delay-related parameters, the delays of the first reflection waveforms, approach those of the forward waveforms. These behaviors of the parameters coincide with the aging effect on the stiffness of the aortic vessels. In the results section, the performance of the model is evaluated by conducting error analysis between the approximated PPWs and the real PPW data. The results show that the maximum relative L_2 error was 5.88% and the maximum AI error was 5.97%. Comparing the errors between two and three decompositions of the approximation model, this study showed that the proposed decomposition model with one forward and two reflected waveforms can play an important role in accuracy of age-related PPWs. Beyond the error analysis, this study demonstrated that the model can recover the FRW from the decomposed waveforms of the PPW without measuring the flow velocity. Moreover, this study reproduced PPWs for a wide range of ages from 15 to 85 years old with an increment of a decade by piecewise-linearly interpolating the parameters of the model. In summary, the effectiveness of the proposed approximation modeling is validated for reconstructing both the PPWs and FRWs based on the hemodynamics of the RAPW at age 85.

REFERENCES

[1] D. A. Duprez, D. R. Kaiser, W. Whitwam, S. Finkelstein, A. Belalcazar, R. Patterson, S. Glasser, and J. N. Cohn, "Determinants of radial artery pulse wave analysis in asymptomatic individuals," *Amer. J. Hypertens.*, vol. 17, no. 8, pp. 647–653, Aug. 2004.

[2] K. Kohara, Y. Tabara, H. Tomita, T. Nagai, M. Igase, and T. Miki, "Clinical usefulness of the second peak of radial systolic blood pressure for estimation of aortic systolic blood pressure," *J. Hum. Hypertens.*, vol. 23, no. 8, pp. 538–545, Jan. 2009.

[3] S. A. Esper and M. R. Pinsky, "Arterial waveform analysis," *Best Pract. Res. Clin. Anaesthesiol.*, vol. 28, no. 4, pp. 363–380, Dec. 2014.

[4] J. Sugawara, K. Hayashi, and H. Tanaka, "Distal shift of arterial pressure wave reflection sites with aging," *Hypertens*, vol. 56, no. 5, pp. 920–925, Sep. 2010.

[5] T. G. Papaioannou, E. N. Karatzis, C. M. Papamichael, K. N. Karatzi, N. A. Zakopoulos, J. P. Lekakis, M. Mavrikakis, and C. Stefanadis, "Circadian variation of arterial pressure wave reflections," *Amer. J. Hypertens.*, vol. 19, no. 3, pp. 259–263, Mar. 2006.

[6] A. Qasem and A. Avolio, "Determination of aortic pulse wave velocity from waveform decomposition of the central aortic pressure pulse," *Hypertension*, vol. 51, no. 2, pp. 188–195, Feb. 2008.

[7] Y. H. Sun, T. J. Anderson, K. H. Parker, and J. V. Tyberg, "Wave-intensity analysis: A new approach to coronary hemodynamics," *J. Appl. Physiol.*, vol. 89, no. 4, pp. 1636–1644, Oct. 2000.

[8] C. J. Jones, M. Sugawara, Y. Kondoh, K. Uchida, and K. H. Parker, "Compression and expansion wavefront travel in canine ascending aortic flow: Wave intensity analysis," *Heart Vessels*, vol. 16, no. 3, pp. 91–98, Mar. 2002.

[9] K. H. Parker, "An introduction to wave intensity analysis," *Med. Biol. Eng. Comput.*, vol. 47, no. 2, pp. 175–188, Feb. 2009.

[10] M. Sugawara, K. Niki, N. Ohte, T. Okada, and A. Harada, "Clinical usefulness of wave intensity analysis," *Med. Biol. Eng. Comput.*, vol. 47, no. 2, pp. 197–206, Feb. 2009.

[11] P. Comon, "Independent component analysis, a new concept?" *Signal Process.*, vol. 36, no. 3, pp. 287–314, Apr. 1994.

[12] A. Hyvärinen and E. Oja, "A fast fixed-point algorithm for independent component analysis," *Neural Comput.*, vol. 9, no. 7, pp. 1483–1492, Mar. 2006.

[13] L. Gbaoui and E. Kaniusas, "Arterial pulse wave decomposition by independent component analysis," in *Proc. IEEE Int. Workshop Med. Meas. Appl.*, Cetraro, Italy, May 2009, pp. 111–115.

[14] L. Gbaoui and E. Kaniusas, "Decomposition of photoplethysmographical arterial pulse waves by independent component analysis: Possibilities and limitations," in *Advances in Biomedical Sensing, Measurements, Instrumentation and Systems*. Berlin, Germany: Springer, 2010, pp. 166–185.

[15] C. Liu, D. Zheng, A. Murray, and C. Liu, "Modeling carotid and radial artery pulse pressure waveforms by curve fitting with Gaussian functions," *Biomed. Signal Process. Control*, vol. 8, no. 5, pp. 449–454, Sep. 2013.

[16] L. Wang, L. Xu, S. Feng, M. Q. Meng, and K. Wang, "Multi-Gaussian fitting for pulse waveform using weighted least squares and multi-criteria decision making method," *Comput. Biol. Med.*, vol. 43, no. 11, pp. 1661–1672, Nov. 2013.

[17] L. Wang, L. Xu, D. Zhao, Y. Yao, and D. Song, "FPGA-based design and implementation of arterial pulse wave generator using piecewise Gaussian-cosine fitting," *Comput. Biol. Med.*, vol. 59, pp. 142–151, Apr. 2015.

[18] S. Laxminarayan, P. Sipkema, and N. Westerhof, "Characterization of the arterial system in the time domain," *IEEE Trans. Biomed. Eng.*, vol. BME-25, no. 2, pp. 177–184, Mar. 1978.

[19] D. S. Berger, J. K. Li, W. K. Laskey, and A. Noordergraaf, "Repeated reflection of waves in the systemic arterial system," *Amer. J. Physiol.*, vol. 264, no. 1, pp. H269–H281, Jan. 1993.

[20] D. S. Berger, J. K. Li, and A. Noordergraaf, "Differential effects of wave reflections and peripheral resistance on aortic blood pressure: A model-based study," *Amer. J. Physiol.*, vol. 266, no. 4, pp. H1626–H1642, Apr. 1994.

[21] B. E. Westerhof, I. Guelen, N. Westerhof, J. M. Karemaker, and A. Avolio, "Quantification of wave reflection in the human aorta from pressure alone: A proof of principle," *Hypertension*, vol. 48, no. 4, pp. 595–601, Aug. 2006.

[22] B. Hametern, S. Wassertheurer, J. Kropf, C. Mayer, A. Holzinger, B. Eber, and T. Weber, "Wave reflection quantification based on pressure waveforms alone–methods, comparison, and clinical covariates," *Comput. Methods Programs Biomed.*, vol. 109, no. 3, pp. 250–259, Mar. 2013.
[23] R. Kelly, C. Hayward, A. Avolio, and M. O'rourke, "Noninvasive determination of age-related changes in the human arterial pulse," *Circulation*, vol. 80, no. 6, pp. 1652–1659, Dec. 1989.
[24] J. U. Kim, S. H. Kim, Y. J. Jeon, H. H. Ryu, Y. J. Lee, H. J. Lee, and J. Y. Kim, "Clinical study of the floating-sinking pulse quantification analysis on ages, left/right, and palpation positions," *J. Physiol. Pathol. Korean Med.*, vol. 23, n. 5, pp. 1193–1198, Oct. 2009.
[25] J. U. Kim, Y. J. Jeon, Y. J. Lee, K. H. Kim, and J. Y. Kim, "Novel diagnostic algorithm for the floating and sunken pulse qualities and its clinical test," *Evid. Based Complement. Alternat. Med.*, 2011, Art. no. 813427.
[26] J. U. Kim, B. Ku, Y. M. Kim, J. H. Do, J. S. Jang, E. Jang, Y. J. Jeon, K. H. Kim, and J. Y. Kim, "The concept of sasang health index and constitution-based health assessment: An integrative model with computerized four diagnosis methods," *Evid. Based Complement. Alternat. Med.*, 2013, Art. no. 879420.
[27] T.-H. Yang, G. Jo, J.-H. Koo, S.-Y. Woo, J.-U. Kim, and Y.-M. Kim, "A compact pulsatile simulator based on cam-follower mechanism for generating radial pulse waveforms," *Biomed. Eng. OnLine*, vol. 18, Jan. 2019, Art. no. 1.
[28] G. F. Mitchell, H. Parise, E. J. Benjamin, M. G. Larson, M. J. Keyes, J. A. Vita, R. S. Vasan, and D. Levy, "Changes in arterial stiffness and wave reflection with advancing age in healthy men and women: The Framingham heart study," *Hypertension*, vol. 43, no. 6, pp. 1239–1245, May 2004.
[29] T. Ashraf, Z. Panhwar, S. Habib, M. A. Memon, F. Shamsi, and J. Arif, "Size of radial and ulnar artery in local population," *J. Pakistan Med. Assoc.*, vol. 60, no. 10, pp. 817–819, Oct. 2010.
[30] R. L. Krullaards, J. J. Pel, C. J. Snijders, and G. J. Kleinrensink, "The potential effects of a biofeedback writing exercise on radial artery blood flow and neck mobility," *Int. J. Biomed. Sci.*, vol. 5, no. 2, pp. 192–197, Jun. 2009.
[31] D. W. E. Schattenkerk, J. van Grop, M. B. Snijder, A. H. Zwinderman, C. O. Agyemang, R. J. G. Peters, and B. J. H. van den Born, "Ethnic differences in arterial wave reflection are mostly explained by differences in body height—Cross-sectional analysis of the helius study," *PLoS One*, vol. 11, no. 7, Jul. 2016, Art. no. e0160243.

GWANGHYUN JO received the B.S., M.S., and Ph.D. degrees from the Department of Mathematical Sciences, KAIST, Daejeon, South Korea, in 2018. From 2018 to August 2019, he was a Postdoctoral Researcher with KAIST. He has been on the faculty of the Department of Mathematics, Kunsan National University, since 2019. His research interests include numerical analysis and simulation of various fluids problems arising from hemodynamics, and petroleum engineering.

TAE-HEON YANG received the B.S. degree from Yonsei University, South Korea, in 2006, and the M.S.E. and Ph.D. degrees from the Department of Mechanical Engineering, Korea Advanced Institute of Science and Technology (KAIST), in 2008 and 2012, respectively. From 2012 to 2017, he was a Senior Research Scientist with the Korea Research Institute of Standards and Science. He has been on the Faculty of Electronic Engineering, Korea National University of Transportation, since 2018. His research includes Haptic sensor and actuator, medical simulator, and human–computer interface.

JAEUK U. KIM received the B.S. degree in physics from POSTECH, South Korea, in 2005, the M.S. degree in physics from the Chalmers University of Technology, Sweden, in 2000, and the Ph.D. degree in physics from the University of Gothenburg, Sweden, in 2005.

Since April 2009, he has been working in the Korea Institute of Oriental Medicine, entered as a Senior Researcher and later promoted to a Principal Researcher. He is also a Professor with the University of Science and Technology (UST). His current interest is in the biosignal analysis and application to the medical technology. His work experience includes electron transport in quantum wires, analysis of human pulse waveform, electrical bio-impedance, electroencephalogram, and eye tracking.

JEONG-HOI KOO received the Ph.D. degree in mechanical engineering from Virginia Tech, in 2003. He is currently a Professor of mechanical and manufacturing engineering with Miami University, Oxford, OH, USA. At Miami University, he is committed to offering high quality teaching to undergraduate engineering students as well as research opportunities to them. He is also committed to engaging engineering students in international education. He has organized and offered serval global educational opportunities and international research experiences for undergraduates. His research focuses on in smart materials and systems. He performs fabrication, testing, modeling, and control research of various smart materials for development of novel actuators and sensors for various engineering applications in mechanical and biomedical systems. Recently, his research activities have extended to Appropriate Technology or Development Engineering. He was elected a Fellow of the American Society of Mechanical Engineers (ASME) in 2019. He is currently serving as an (Associate) Editor for the *Journal of Vibration and Control*, the *Shock and Vibration Journal*, and *Frontiers in Materials—Smart Materials*.

YOUNG-MIN KIM received the B.S. degree in mechanical engineering from Yonsei University, Seoul, South Korea, in 1999, the M.S. degree in mechanical engineering from POSTECH, South Korea, in 2001, and the Ph.D. degree in mechanical engineering from KAIST, South Korea, in 2011. From 2002 to 2006, he was a Research Scientist with the Human-Welfare Robotic System Research Center, KAIST. Since 2011, he has been a Principle Researcher with the Future Medicine Division, Korea Institute of Oriental Medicine, South Korea. His research interest includes the medical devices for the personalized healthcare, wearable sensors for daily health monitoring, sophisticated human–robot interface (HRI) technology, and innovative HRI applications.